Bulletin of the Geological Society of Finland, Vol. 77, 2005, pp. 129–150

Supracrustal rocks in the Kuovila area, Southern Finland: structural evolution, geochemical characteristics and the age of volcanism

Pietari Skyttä*, Asko Käpyaho & Irmeli Mänttäri
Geological Survey of Finland, P.O. Box 96, FI-02151 Espoo, Finland

Abstract

The supracrustal rocks of the Kuovila area in the Palaeoproterozoic Svecofennian Uusimaa Belt, southern Finland, consist mainly of volcaniclastic rocks associated with banded iron formations (BIFs) and marbles. Small ZnS and PbS mineralizations are occasionally located within the marbles. Some primary features are well preserved in the sedimentary and volcanic rocks, including lamination in tuffites and banded iron formations.

Geochemical results show that the volcanism was bimodal and it mainly had volcanic arc affinity. Specific geochemical indicators suggesting a volcanic arc origin for the Kuovila volcanic rocks include: 1) Enrichment of LILE over the HFSE elements and 2) Distinctly low Nb and Ta contents in relation to Th, Ce and LREE. Geochemistry of the Kuovila area volcanic rocks is very similar to those of the Orijärvi and Kisko formations, located ~15 km NE of Kuovila.

Felsic tuff in the Kuovila area was dated at 1891±4 Ma by the U-Pb system on zircons. Consequently volcanism was contemporaneous with magmatism in the adjacent Orijärvi area, thus representing the earliest identified volcanic stage in the southern Svecofennian Uusimaa Belt.

Early deformation structures within the Kuovila area are suggested to relate to low-metamorphic or localized low-angle thrusting during D_1. F_1 folds were recumbent and the S_1 cleavages are generally weak. Thrusting was followed by approximately N–S contraction with upright, peak-metamorphic F_2 folding overprinting D_1 structures and defining the Kuovila synform. Two separate intrusive phases include a synvolcanic granodiorite-diorite-gabbro association and a weakly S_2-foliated syn-D_2 granodiorite. Anatectic granites and associated migmatizing veins are absent, therefore suggesting that D_2 pre-dates the ~1.84–1.82 Ga metamorphic event in the Southern Svecofennian Arc Complex (SSAC). D_2 structures in the Kuovila area are suggested to correlate with the early structures with associated axial planar cleavages in the Orijärvi area. D_2 strain is localized into axial planar high strain zones and the curvilinear patterns of the B_2 fold axes probably result from vertical stretching during D_2.

Keywords: supracrustals, metavolcanic rocks, igneous rocks, geochemistry, deformation, structural geology, volcanism, Palaeoproterozoic, Kuovila, Finland

* Corresponding author email: pietari.skytta@gtk.fi

1. Introduction

The Kuovila area is located in the Palaeoproterozoic Svecofennian ~1.90–1.80 Ga supracrustal Uusimaa Belt, southern Finland (Fig. 1), 12 km SW of the Orijärvi area, known for its Cu-Zn-Pb-mineralizations (e.g. Mäkelä, 1989) and as the area in which Eskola (1915) first developed the metamorphic facies concept. The Uusimaa Belt consists of bimodal volcanic rocks, metapelites and metagraywackes (Simonen, 1953; Koistinen, 1992), massive sulphide deposits (Latvalahti, 1979), marbles (Reinikainen, 2001) and banded iron formations (Keinänen, 1980; Sipilä, 1981). Similar lithologies and ore deposits are typical of the Bergslagen area in south-central Sweden (Lundström & Papunen, 1986; Allen et al., 1996) and for that reason these two supracrustal belts are often correlated (Ekdahl, 1993; Nironen, 1997).

The age of volcanism in the Uusimaa Belt has recently been constrained rather well; conventional U-Pb age on zircons from felsic volcanic rocks at Norrlammala, 35 km WSW of Kuovila, is 1888±11 Ma (Reinikainen, 2001). Väisänen & Mänttäri (2002) showed that the age of volcanism is 1895±3 Ma in the Orijärvi formation, lowermost in the Orijärvi area stratigraphy, and 1878±4 Ma in the Kisko formation, overlying the Orijärvi formation. Ages for intrusive rocks from the Uusimaa Belt include a quartz diorite at 1891±13 Ma (Huhma, 1986) and granodiorites at Orijärvi at 1898±4 Ma (Väisänen et al., 2002) and at 1891±13 Ma (Huhma, 1986), and have been considered synvolcanic (e.g. Colley & Westra, 1987; Väisänen & Mänttäri, 2002). A discordantly cutting gabbroidic pegmatite in the southern part of the SSAC is dated at 1885±7 Ma, setting a minimum age for the volcano-sedimentary rocks and a maximum age for the first deformation phase with associated penetrative metamorphic fabric (Hopgood et al., 1983). The lateorogenic granitoids of the southern Svecofennian domain are generally anatectic S-type microcline granites (Nironen, 2003) and mostly indicate ages between 1.82 and 1.84 Ga (Huhma, 1986; Suominen, 1991; Kurhila et al., 2004), thus being concurrent with the peak of the younger metamorphic event (Mouri et al., 2005). In addition, a younger, A-type resembling granite crosscutting the surrounding migmatites at Karjaa yielded an age of 1826±11 Ma (Jurvanen et al., 2005).

Analysis of strain and kinematic history in a polydeformed, highly migmatized region, such as the Svecofennian domain of southern Finland, is particularly difficult due to destruction of early structures at high-grade metamorphic events, associated migmatization and multiple intrusive events. Resolution of the original tectonic environment of these rocks, their geometry and kinematic history, and the relationship between deformation, magmatic events and metamorphism provide important constraints on understanding the Svecofennian orogeny. As a non-migmatized area with preserved deformation structures related to

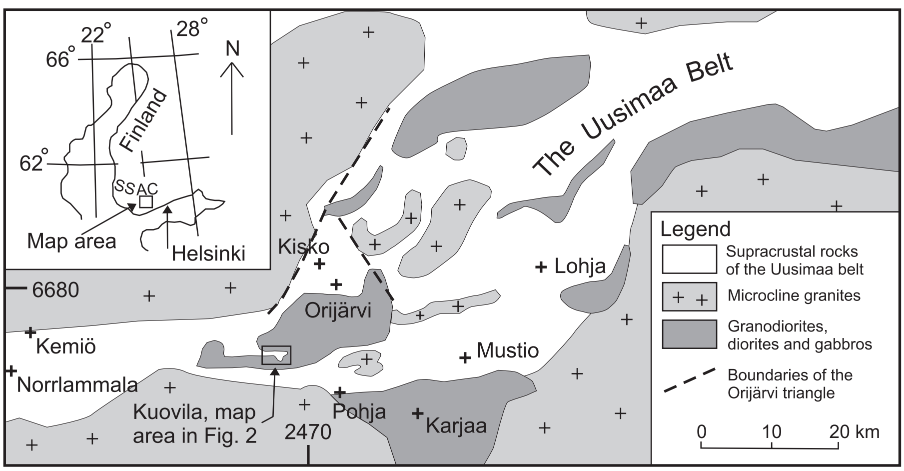

Fig. 1. Geological setting of the Kuovila area. Simplified after Schreurs &Westra (1986). SSAC = Southern Svecofennian Arc Complex of Väisänen et al. (2002).

the earliest stages of the tectono-metamorphic history of the SSAC, the Kuovila area provides an opportunity for this. In particular, some constraints on spatial strain variations and kinematic constraints of the main deformational events may be suggested. Also the primary geochemical affinities of the volcanic rocks in the Kuovila area were studied, and combined with the tectonic evolution and the new U-Pb age determination they provide information on the probable tectonic setting of the volcanism during the Svecofennian orogenesis.

2. Geological setting

Eskola et al. (1919) compiled the first geological map for the Kuovila area, after having previously described igneous and pyroclastic rocks (Eskola, 1914). Later on, Tavela (1950) produced a geological map of Kuovila area with stratigraphical and structural interpretations. Tuominen (1957) published a geological map of the Orijärvi area with a further structural interpretation. Käpyaho (2001) studied the area with particular emphasis on the preserved primary structures and geochemical characteristics.

The Svecofennian domain collided against the Archean continent at 1.910–1.885 Ga (Korsman et al., 1999), whereafter the Uusimaa Belt rocks were deformed and metamorphosed episodically (Nironen, 1997) or semicontinuosly (Gorbatshev & Bogdanova, 1993) during the Svecofennian orogeny, at ca. 1.89 to 1.80 Ga. Two metamorphic events with associated migmatization took place between 1.885–1.810 Ga in the Southern Svecofennian Arc Complex (SSAC, cf. Väisänen et al., 2002). The older event is bracketed between U-Pb ages at 1882±6 Ma and 1877±6 Ma on sphenes and monazites, respectively (Hopgood et al., 1983). The younger event is characterized by high-temperature, low-pressure (HTLP) conditions (Korsman et al, 1999), P estimates ranging from 3 to 5 kbar and T from 550°C to 825°C (Schreurs & Westra, 1986), thus locally reaching granulite facies conditions. Peak metamorphic conditions of the younger event prevailed at ~1.830–1.815 Ga (Levin et al., 2005; Mouri et al., 2005).

The tectonic setting and the depositional environment of the Uusimaa Belt rocks have been discussed in several papers; the belt being interpreted as a palaeo-island arc (e.g. Hietanen, 1975; Latvalahti, 1979; Mäkelä, 1989; Gáal, 1990; Ploegsma & Westra, 1990) or a back-arc basin (e.g. Colley & Westra, 1987; Nironen, 1997). Väisänen & Mänttäri (2002) described the Orijärvi area as resembling a modern volcanic arc with back-arc basin, and identified the progressive development of geochemical characteristics in the volcanic rocks, starting with bimodal magmatism and evolving to intermediate compositions after 10–15 Ma.

Previous structural studies have identified two (Ehlers et al., 1993), three (Shreurs & Westra, 1986; Bleeker & Westra, 1987; Ploegsma & Westra, 1990) or four deformation phases (Verhoef & Dietvorst, 1980; van Staal & Williams, 1983; Kilpeläinen & Rastas, 1990; Levin et al., 2005) in the SSAC. The early deformation phases are suggested to be thrust-related recumbent folds, while the interpreted tectonic transport directions are variable (Ehlers et al., 1993; van Staal & Williams, 1983). Ehlers et al. (1993) defined two recumbent fold sets: the first set (D_1) deformed the 1.89–1.88 Ga granitoids and the second (D_2) set deformed also the 1.84–1.83 Ga microcline granites, thereafter transitioning into upright folding. Generation of the 1.84–1.81 Ga microcline granites is suggested to predate the end of recumbent F_1 folding (Shreurs & Westra, 1986) and the early stage of the recumbent, thrust-related D_2 of Ehlers et al. (1993). Thus, it also predates the peak metamorphic main folding, characterized by E–W trending upright folds (Schreurs & Westra, 1986; Bleeker & Westra, 1987; Ploegsma & Westra, 1990; Levin et al., 2005). In addition, Ploegsma & Westra (1990) recognized the Orijärvi triangle as a non-migmatized low tectonic strain area with preserved early deformation structures.

2. Description of the rock units

2.1. Supracrustal rocks

In the Kuovila area, metamorphosed, non-migmatitic volcaniclastic deposits, principally tuffs and tuffites dominate the supracrustal rocks (Fig. 2). Tuffs are

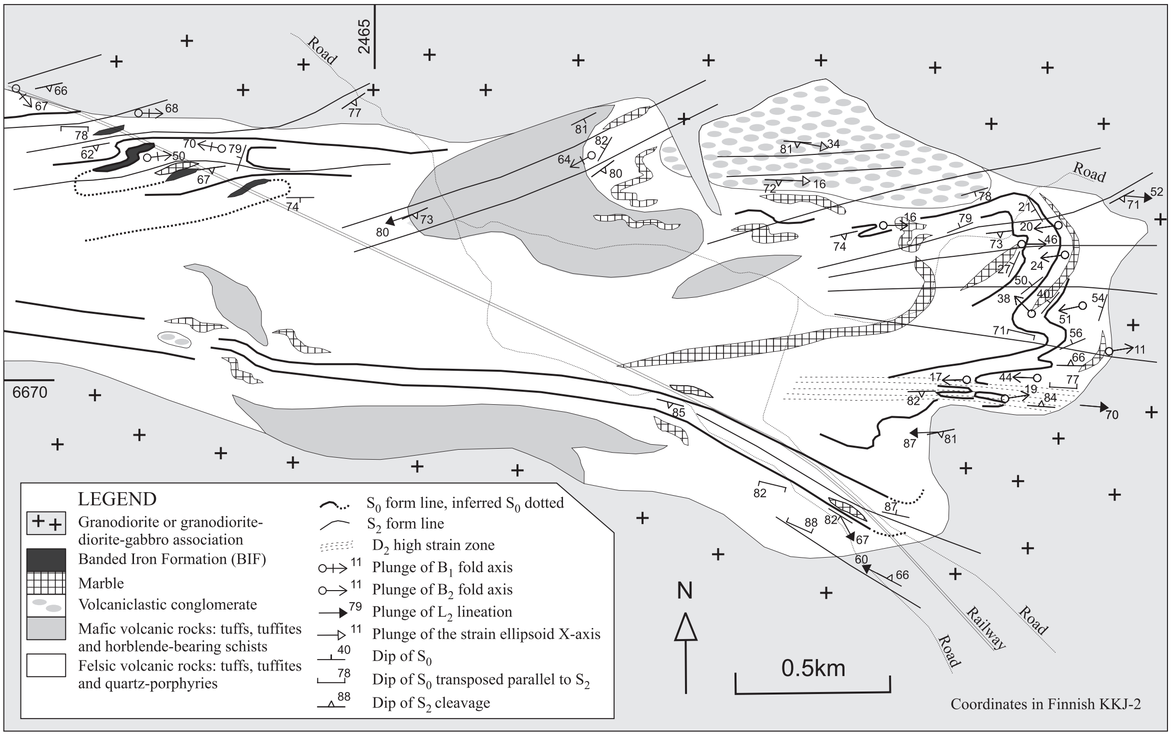

Fig. 2. Geological map of the Kuovila area. Lithology modified after Käpyaho (2001).

composed of purely volcanic material, whereas tuffites are redeposited and contain also sedimentary material. Tuffs and tuffites are bimodal (mafic and felsic), often fine-grained and usually preserve primary bedding (S_0), including fine lamination, throughout much of the area. Layers are commonly from 2 cm to a few meters thick. Tuffs and tuffites occasionally have quartz porphyry interlayers with polycrystalline and anhedral quartz from a few mm to 1 cm in diameter. Interbeds of calcitic marble and BIF are present within the volcanic rocks. Mafic plagioclase-phyric tuffites and tuffs, as well as schistose layers of even-grained hornblende-bearing tuffs, later here called hornblende schists, are also present. In general, the felsic compositions are more common and the intermediate volcanic rocks are rare.

An unstratified volcaniclastic conglomerate horizon is located in the northern part of the study area. It shows a bimodal composition, with the fragments being felsic and the fine-grained matrix mafic (Tavela, 1950). Fragment size distribution ranges from less than 1 mm to more than 12 cm, with an average of 1 cm. Felsic fragments are rounded, variably elongated due to localized strain, and sometimes show weak zoning. Furthermore, microscopic observations reveal angularity of the fragments. Rounded calcite cavities, reaching 10–20 cm in diameter are also found within the conglomerate.

Sedimentary rocks include marbles and banded iron formations (BIFs). The marbles consist mainly of medium- to coarse-grained calcite. Fine-grained grey dolomite is quite rare. Layering and lamination are the only observed primary structures of the marbles. Rare small sphalerite bands and pods, with occasional galena, are present in marbles near the volcaniclastic conglomerate unit. Skarn formations with diopside, epidote and zoisite are locally present at contact with the marbles and as interlayers within tuffs and tuffites.

Banded iron formations are associated mainly with felsic, fine-grained, laminated tuffs and tuffites and in few places with quartz porphyries. Thicknesses of BIF units generally range from 2 to 10 m. They are thin-bedded and laminated, consist principally of separate bands of magnetite, quartz, garnet, and actino-

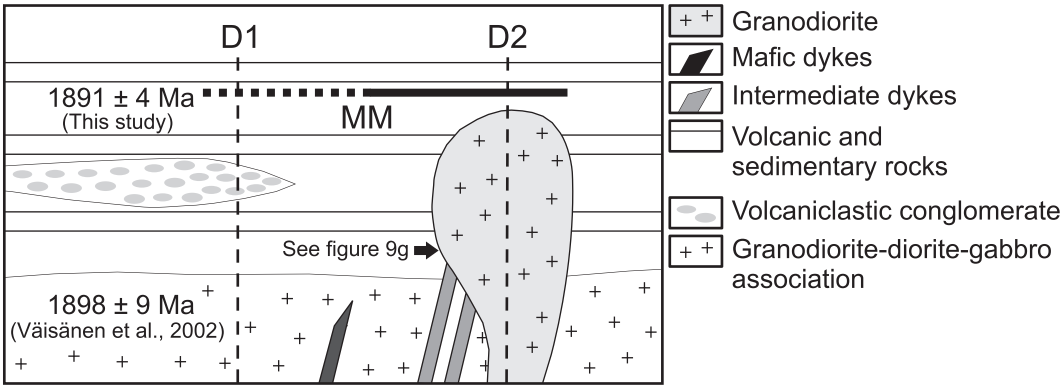

Fig. 3. Crosscutting relationships of the dykes, intrusive and supracrustal rocks relative to deformation and metamorphism (MM) in the Kuovila area.

lite. Calcite and dolomite are only present as accessory minerals.

2.3. Intrusive rocks and dykes

Two separate intrusive suites have been identified (Fig. 3). 1) A synvolcanic granodiorite-diorite-gabbro association (cf. Väisänen et al., 2002) has intense tectonic foliation (foliation used for tectonic orientation in the intrusive rocks) and commonly contains mafic magmatic enclaves (MME), whose magmatic origin is established by felsic xenocrysts within the enclaves. The contact relationship between the rocks of this association and the supracrustal rocks of the Kuovila area is, however, not found. 2) A separate, weakly S_2 -foliated granodiorite intrudes layered volcanic rocks in the F_2 fold hinge and along the F_2 axial plane, thus being syntectonic with D_2. It has a steep quartz aggregate lineation and contains very few MMEs. Microcline granites characteristic for the SSAC are absent.

Mafic plagioclase-phyric dykes and sills, from 10 to 50 cm wide, often cut the tuffs and tuffites, whereas fine- and even-grained mafic dykes are found to cut the synvolcanic intrusive association. The mafic dykes have a rather uniform orientation and pre-date one major folding event (D_2). One suite of intermediate dykes comprising an S_2 cleavage occurs in the hinge of the F_2 folds, and is cut by the weakly S_2-foliated granodiorite. Other intermediate dykes suggest emplacement prior to D_1, but may, however, not be reliably correlated with deformation events. The intermediate dykes are variably porphyritic in general.

3. Geochemistry

3.1 Samples and methods

Samples for the geochemical analysis were collected from representative rock units, least affected by secondary alteration. Crushing of the samples was made with manganese steel jaw crusher and grinding in carbon steel and tungsten carbide grinding vessels for X-ray fluorescence (XRF) and inductively-coupled plasma mass spectrometry (ICP-MS), respectively. The decomposition of the samples was carried out in two steps: dissolution with hydrofluoric-perchloric acid and making fusion of the undissolved sample with lithium metaborate/sodium perborate. Major elements and Sr, Cr, Ni, Cu, Zn, Ga, Ba and Pb were determined by XRF on powder pellettes whereas total concentrations the other trace elements (Rb, Th, U, Nb, Zr, Y, Hf, Sc, Ta, V, La, Ce, Pr, Nd, Sm, Eu, Gd, Tb, Dy, Ho, Er, Tm, Yb and Lu) were analysed with ICP-MS at the Geological Survey of Finland. Results and the sample coordinates are presented in Table 1.

3.2 Whole-rock geochemistry

Major elements

In the total alkali vs. silica –diagram all the Kuovila rocks show a bimodal character (Fig. 4a). Exceptions

Table 1. Chemical composition of the Kuovila rocks

Sample	R408	R405	R409	AAK-00-	R404	R408	R412	R412	R413	AAK-00-	AAK-00-	AAK-00-	R408	AAK-00-	AAK-00-	AAK-00-	R406
	3.80	60.15	73.10	51	8.50	48.70	17.60	95.00	33.20	26	97	113	62.00	17	49	60a	38.00
Rock type	Qtz	Qtz	Qtz	Qtz	Hbl	Hbl	Hbl	Hbl	Hbl	Hbl	Hbl	Hbl schist	Lam.	Lam.	Lam.	Lam.	Fels.
	porph	porph	porph	porph	schist	schist	schist	schist	schist	schist	schist		tuffite	tuffite	tuffite	tuffite	tuff/-ite
SiO_2 (wt%)	74.7	75.6	74.4	74.6	49.7	42.4	51.1	54.1	53.6	49.8	50.5	51.9	76.8	71.5	70.9	70.3	67.2
TiO_2	0.151	0.273	0.157	0.262	1.24	0.601	0.687	1.36	1.27	0.800	0.746	0.803	0.314	0.376	0.178	0.421	0.488
$Al2O_3$	11.9	11.9	12.0	12.4	15.1	11.4	16.1	15.4	14.5	14.3	15.0	15.1	10.2	12.5	10.5	13.7	12.6
$Fe2O_3$	2.23	1.97	2.39	3.66	12.5	13.5	8.62	7.67	12.4	14.8	12.9	10.8	3.18	4.25	3.32	2.68	5.92
MnO	0.032	0.038	0.036	0.074	0.216	0.244	0.204	0.117	0.205	0.222	0.232	0.175	0.043	0.083	0.084	0.039	0.132
MgO	0.72	0.77	0.62	0.34	4.38	12.2	4.21	4.07	3.10	4.37	4.34	4.68	1.88	1.58	4.02	3.20	2.74
CaO	0.864	1.42	1.06	2.66	8.97	11.6	11.3	6.53	8.13	9.71	8.83	8.89	1.45	4.19	8.27	3.65	5.52
Na_2O	1.15	1.71	0.96	3.93	4.10	1.71	3.33	3.69	4.13	2.20	3.14	3.83	3.19	2.44	0.44	2.93	1.96
K2O	6.81	5.52	6.85	1.29	0.446	0.659	0.908	1.52	0.210	0.591	0.762	0.654	1.76	1.37	0.949	1.76	1.51
P2O5	0.012	0.025	0.016	0.052	0.303	0.203	0.146	0.478	0.370	0.140	0.071	0.156	0.055	0.065	0.055	0.105	0.091
Total	98.6	99.2	98.5	99.3	96.9	94.5	96.6	95.0	97.9	96.9	96.6	96.9	98.9	98.3	98.7	98.8	98.2
Rb (ppm)	176	89.4	155	31.1	4.71	5.43	25.9	54.5	4.64	4.61	9.83	6.81	56.8	56.2	27.1	119	34.2
Ba	2463	1976	2489	686	354	97	29	457	284	194	16	188	175	687	80	254	505
Th	16.7	17.5	15.7	7.86	1.60	b.d.l	4.81	2.95	5.69	1.38	1.60	5.64	11.0	14.7	11.6	8.84	10.5
U	7.61	6.16	6.83	2.47	1.09	b.d.l	2.09	1.57	2.30	0.92	1.08	2.23	5.31	4.11	4.42	2.67	5.02
Nb	11.7	20.7	11.0	9.93	3.98	5.14	6.62	15.0	4.68	2.63	2.54	3.19	12.4	14.5	11.6	13.0	10.3
Sr	48	81	52	128	239	111	188	1042	228	24	188	233	79	229	45	99	126
Zr	178	446	165	165	55.9	35.3	89.0	126	80.8	54.0	45.8	59.7	173	312	208	263	178
Y	45.9	66.1	46.4	34.2	16.3	12.2	23.2	10.7	25.4	20.9	12.9	15.7	24.9	40.8	50.7	49.9	36.0
Hf	4.95	11.2	4.87	4.41	1.22	0.80	2.28	2.69	2.07	1.36	1.06	1.41	3.86	7.54	5.36	6.23	4.32
Sc	8.20	8.14	7.85	12.3	40.8	41.5	33.6	15.3	37.6	55.9	53.5	41.5	7.28	10.9	6.56	13.1	16.1
Ta	0.95	1.38	0.88	0.79	0.29	0.31	0.52	0.85	0.37	b.d.l	b.d.l	0.22	0.95	0.80	1.00	1.01	0.79
V	3.67	1.91	1.86	6.45	279	163	201	135	221	398	389	262	9.04	15.5	3.55	28.2	80.1
Cr	6	12	9	12	45	1088	46	48	7	23	41	76	6	6	10	10	10
Ni	3	0	0	5	16	269	21	37	3	16	9	33	0	6	5	0	0
Cu	7	2	24	10	45	6	64	33	5	37	77	0	20	17	0	24	0
Zn	335	18	62	102	146	209	85	99	103	174	132	78	43	60	62	82	163
Ga	27	23	24	19	21	19	28	23	20	23	24	21	16	26	18	24	26
Pb	58	23	45	16	39	14	22	21	47	20	42	12	21	26	15	35	24
La	42.9	53.0	38.9	4.49	10.5	4.90	18.5	35.8	21.7	9.76	4.39	13.9	34.9	29.3	39.8	21.7	35.6
Ce	85.1	110	77.3	15.9	23.7	12.9	39.1	75.5	47.8	23.1	12.7	29.4	68.2	64.4	79.3	49.9	71.5
Pr	9.16	12.6	8.62	1.40	2.84	1.85	4.43	8.78	5.61	3.11	1.85	3.44	7.67	6.80	9.04	6.08	8.23
Nd	36.3	54.4	33.5	6.35	13.0	9.69	19.1	38.1	24.5	15.5	8.66	14.0	28.4	27.0	37.5	24.5	32.2
Sm	7.24	11.3	6.57	2.13	2.79	2.20	3.84	5.42	4.91	3.46	2.24	2.96	4.84	5.59	6.87	5.62	5.65
Eu	0.75	1.76	0.84	0.64	1.04	0.75	1.11	1.66	1.42	0.94	0.73	0.88	0.70	1.27	0.74	1.00	1.00
Gd	7.24	11.3	7.01	3.33	3.25	2.64	3.91	4.35	5.24	3.73	2.46	3.06	5.19	5.91	8.13	6.22	6.19
Tb	1.21	1.79	1.06	0.66	0.45	0.39	0.64	0.53	0.80	0.58	0.36	0.48	0.76	1.04	1.35	1.18	0.93
Dy	7.44	10.6	6.73	4.69	2.70	2.16	3.92	2.29	4.38	3.35	1.96	2.57	4.04	6.70	7.99	8.35	5.54
Ho	1.56	2.15	1.47	1.11	0.59	0.43	0.79	0.39	0.88	0.68	0.45	0.55	0.84	1.31	1.47	1.74	1.19
Er	5.00	6.43	4.60	3.51	1.70	1.27	2.10	0.88	2.40	2.18	1.28	1.47	2.20	3.84	4.44	5.03	3.54
Tm	0.75	1.02	0.72	0.58	0.27	0.18	0.35	0.12	0.39	0.34	0.22	0.26	0.37	0.59	0.75	0.84	0.49
Yb	5.31	6.67	4.93	4.07	1.47	1.22	2.32	0.64	2.45	1.99	1.46	1.45	2.37	3.9	4.79	5.05	3.62
Lu	0.81	0.96	0.77	0.59	0.26	0.15	0.32	b.d.l	0.39	0.31	0.16	0.24	0.37	0.61	0.70	0.75	0.52
Northing	6670358	6670586	6670300	6670639	6670345	6670358	6670212	6670212	6670215	6670628	6670801	6670007	6670358	6670136	6670486	6670582	6670453
Easting	2466956	2467085	2466959	2466393	2467302	2466956	2466961	2466961	2466542	2466805	2465965	2465925	2466956	2467172	2466348	2466403	2466958

b.d.l = below detection limit. Coordinates in Finnish KKJ-2. Abbreviations: Qtz porph = quartz porphyry, Hbl schist = even-grained mafic tuffs and tuffites (hornblende schists), Lam. tuffite = Felsic laminated tuffite, Fels. tuff/-ite = Felsic tuffs and tuffites, Volcaniclast. = volcaniclastic conglomerate, Plg-phyric = plagioclase-phyric tuffs and tuffites. Down hole depth of drill core sample indicated after sample id (meters), e.g. R408 3.80. XRF data from Käpyaho (2001)

Table 1. continued

Sample	R407 52.10	R407 84.00	R414 58.70	AAK-00-48	AAK-01-01	AAK-01-12	AAK-00-95	R404 22.35	R405 52.00	R409 44.20	R410 101.80	R412 10.10	R412 40.80	R413 110.10	AAK-00-1	AAK-00-73
Rock type	Fels. tuff/-ite	Fels. tuff/-ite	Fels. tuff/-ite	Fels. tuff/-ite	Volcani-clast.	Volcani-clast.	Volcani-clast.	Plg-phyric	Plg-phyric	Plg-phyric	Plg-phyric	Plg-phyric	Plg-phyric	Plg-phyric	Plg-phyric	Plg-phyric
SiO2 (wt%)	68.7	67.6	69.5	69.4	59.6	70.5	62.7	48.5	54.3	55.9	44.2	54.3	50.4	48.7	49.7	54.8
TiO2	0.405	0.379	0.788	0.358	0.783	0.348	0.718	0.813	1.38	0.870	1.03	0.601	0.591	0.464	0.668	0.563
Al2O3	14.0	11.9	16.8	15.7	14.1	14.2	13.6	19.1	16.3	16.3	13.9	14.1	17.8	17.1	15.2	17.3
Fe2O3	5.68	5.96	1.18	1.40	9.06	4.34	7.63	10.1	7.95	10.4	12.0	10.4	9.86	10.3	13.0	8.95
MnO	0.109	0.128	0.035	0.020	0.181	0.073	0.136	0.175	0.082	0.211	0.188	0.185	0.159	0.155	0.216	0.158
MgO	0.95	3.59	0.41	1.39	2.52	1.09	2.11	3.91	4.08	3.01	9.75	4.89	5.18	5.49	4.46	3.08
CaO	4.06	4.53	3.82	3.34	6.73	2.20	5.77	10.1	7.03	7.09	10.6	8.69	10.0	10.1	8.25	7.81
Na2O	3.74	2.39	4.44	1.31	3.50	4.27	3.54	3.12	3.72	2.27	1.71	2.14	1.93	3.09	3.12	3.14
K2O	1.32	1.62	2.40	5.61	2.27	2.26	2.12	0.582	1.62	1.15	1.16	1.03	1.15	0.922	1.46	0.907
P2O5	0.116	0.064	0.200	0.062	0.162	0.072	0.140	0.161	0.467	0.206	0.150	0.115	0.136	0.082	0.147	0.184
Total	99.1	98.2	99.5	98.6	98.9	99.3	98.4	96.7	97.0	97.4	94.7	96.5	97.2	96.4	96.2	96.9
Rb (ppm)	34.0	40.8	42.1	196	62.8	62.2	47.8	13.4	44.9	38.5	29.7	34.0	35.0	39.0	62.3	28.1
Ba	433	672	298	323	489	672	498	182	531	211	197	219	173	229	395	175
Th	7.18	15.0	8.28	13.9	7.37	7.65	6.64	0.58	2.96	2.96	0.61	2.15	0.61	1.26	1.69	1.15
U	3.51	5.69	3.69	4.61	2.97	4.00	3.09	0.54	1.34	1.80	0.27	1.28	0.46	0.70	1.49	0.86
Nb	7.32	20.4	7.25	14.2	9.01	5.53	7.79	2.02	13.8	3.27	3.51	3.96	1.74	1.80	2.40	1.85
Sr	205	119	416	69	114	111	93	412	116	317	27	179	331	273	178	341
Zr	127	273	185	312	159	116	146	30.4	141	66.3	41.4	65.8	27.3	35.4	36.3	39.5
Y	28.2	59.9	26.3	36.1	26.5	15.6	30.6	11.5	9.52	21.7	16.9	18.8	9.30	9.96	11.6	12.7
Hf	3.20	6.97	4.47	7.31	3.86	3.02	3.61	0.69	2.72	1.57	1.09	1.53	0.81	0.85	1.67	1.02
Sc	16.8	10.4	13.6	12.9	25.6	14.7	22.0	36.2	15.8	36.0	35.3	47.3	32.5	45.3	40.5	31.1
Ta	0.57	1.45	0.52	0.91	0.61	0.58	0.63	b.d.l	0.80	0.25	0.26	0.29	b.d.l	b.d.l	0.43	b.d.l
V	43.6	31.8	84.4	6.96	159	52.1	145	271	134	178	279	213	210	266	311	154
Cr	11	10	8	2	10	9	6	26	48	4	399	167	95	69	11	11
Ni	0	6	3	4	6	1	7	16	36	0	137	26	29	19	21	7
Cu	18	7	10	4	7	36	10	61	57	14	13	23	40	88	45	58
Zn	75	162	37	51	124	59	136	105	68	130	98	111	102	87	140	1316
Ga	19	26	19	25	22	17	20	23	22	27	19	20	21	18	25	20
Pb	24	34	157	62	23	32	41	25	18	18	16	22	16	22	23	385
La	24.8	52.3	17.1	21.4	15.4	18.4	19.8	6.24	31.8	12.5	4.79	11.8	6.75	6.55	2.56	10.1
Ce	48.9	111	35.6	42.7	43.1	33.6	41.1	13.9	71.4	27.3	13	26.4	14.5	11.8	8.39	21.8
Pr	5.53	12.6	4.31	4.74	4.42	3.58	5.20	1.88	8.86	3.42	1.82	3.31	1.95	1.55	1.39	2.76
Nd	24.1	52.4	19.2	18.8	18.8	13.8	22.8	9.87	35.4	17.4	8.94	14.9	9.42	7.19	7.57	12.1
Sm	4.82	10.0	4.51	3.65	4.25	2.59	4.63	2.31	5.07	3.70	2.56	2.94	1.97	1.58	2.56	2.26
Eu	1.01	1.66	1.07	1.11	1.00	0.63	1.01	0.85	1.50	1.22	0.90	0.77	0.61	0.57	0.85	0.76
Gd	5.08	10.3	4.61	3.95	4.36	2.54	4.95	2.29	4.12	4.51	3.06	3.33	1.72	1.96	2.55	2.45
Tb	0.75	1.61	0.72	0.70	0.72	0.39	0.79	0.34	0.46	0.60	0.45	0.50	0.27	0.27	0.46	0.38
Dy	4.35	9.99	4.40	5.14	4.53	2.33	4.96	1.98	1.99	3.33	2.77	2.96	1.59	1.49	2.72	2.21
Ho	0.93	2.03	0.85	1.22	0.94	0.46	1.03	0.40	0.32	0.71	0.59	0.62	0.30	0.32	0.53	0.45
Er	2.73	5.69	2.91	3.83	2.79	1.50	3.00	1.26	0.72	2.00	1.56	1.86	1.01	0.93	1.91	1.41
Tm	0.42	0.95	0.42	0.66	0.41	0.23	0.57	0.18	0.12	0.30	0.22	0.28	0.11	0.15	0.38	0.20
Yb	2.79	6.04	2.65	4.73	2.75	1.64	3.24	1.19	0.68	2.04	1.70	1.86	0.72	0.97	1.79	1.35
Lu	0.39	0.88	0.40	0.72	0.45	0.25	0.43	0.16	b.d.l	0.26	0.21	0.30	0.11	0.14	0.34	0.19
Northing	6670408	6670408	6670487	6670481	6670762	6670724	6670762	6670345	6670586	6670300	6670255	6670212	6670212	6670215	6670258	6670000
Easting	2466958	2466958	2466690	2466289	2466275	2463401	2466100	2467302	2467085	2466959	2466959	2466961	2466961	2466542	2467075	2466854

Coordinates in Finnish KKJ-2

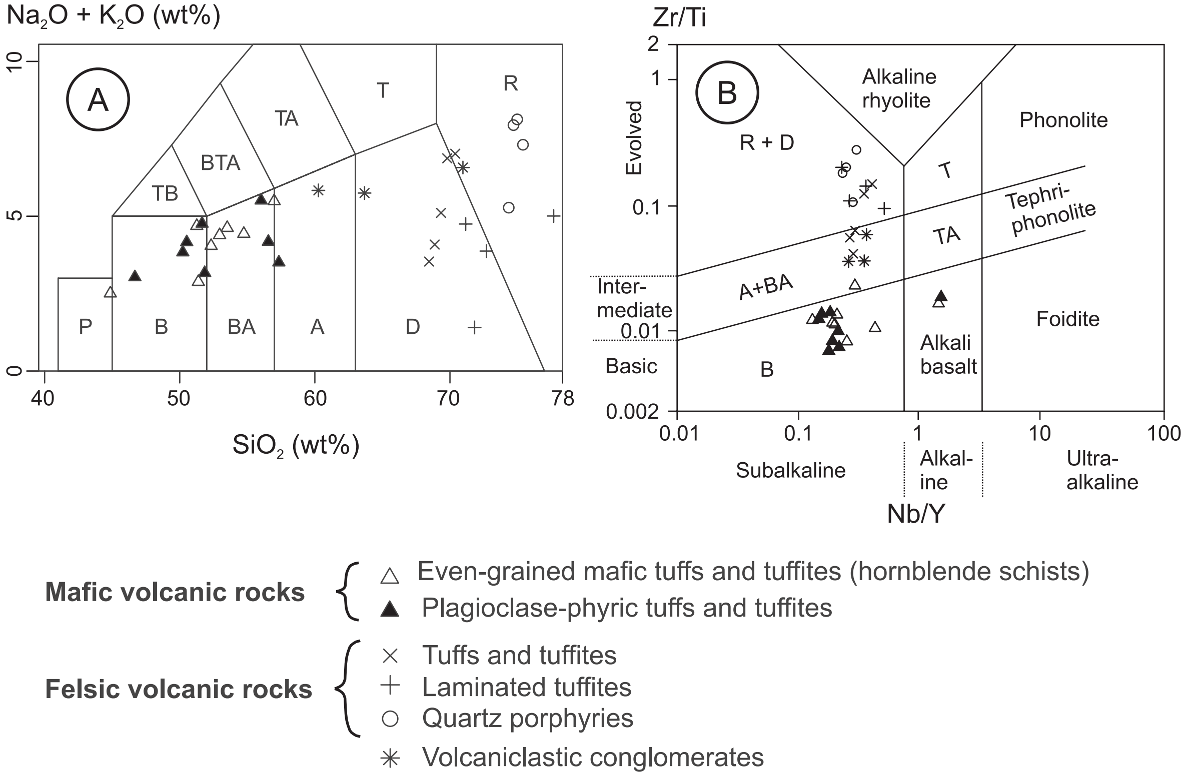

Fig. 4. a) Total alkali vs. SiO_2 (TAS) diagram. Fields after Le Bas et al. (1986). P = Picrobasalt, B = Basalt, BA = Basaltic andesite, A = Andesite, D = Dacite, TB = Trachybasalt, BTA = Basaltic trachyandesite, TA = Trachyandesite, T = Trachyte, R = Rhyolite. b) Zr/Ti vs. Nb/Y diagram after Pearce (1996). Fields as in A).

to this are two of the sampled volcaniclastic conglomerates whose bulk compositions are intermediate, reflecting the bimodal composition of the rock, with a mafic matrix and felsic fragments. Plagioclase-phyric tuffs and tuffites and hornblende schists form a homogenous group within basaltic and basaltic andesite fields with one sample in the picrobasalt field. Felsic tuffs and tuffites, laminated tuffites as well as quartz poprhyries plot in the dacite and rhyolite fields. The rhyolitic quartz porphyry samples show a wide range from low-K to mainly shoshonitic compositions (Fig. 5). All the other samples plot within the medium-K field. Immobile element Zr/Ti vs. Nb/Y plot after Pearce (1996) (Fig. 4b) also indicates bimodal character of the samples with clusters both in the basalt and in the rhyolite + dacite fields. Similar to the TAS diagram is also the intermediate bulk composition of the volcaniclastic conglomerates. Majority of the samples plot in the subalkaline field (Fig. 4b). For comparison, compositional fields of the major elements of the Orijärvi formation samples are shown in Figure 5. A distinct similarity exists between these two areas. Orijärvi formation samples form slightly tighter groupings compared to the Kuovila samples, while the K-content variation of the quartz porphyry samples of this study most probably indicates alteration.

Trace elements

Multi-element spider diagrams, chondrite-normalized rare earth element (REE) diagrams and a discrimination diagram by Wood et al. (1979) is shown in order to present the trace element contents of the studied samples. Abbreviations used in the text are large ion lithophile element (LILE), high field

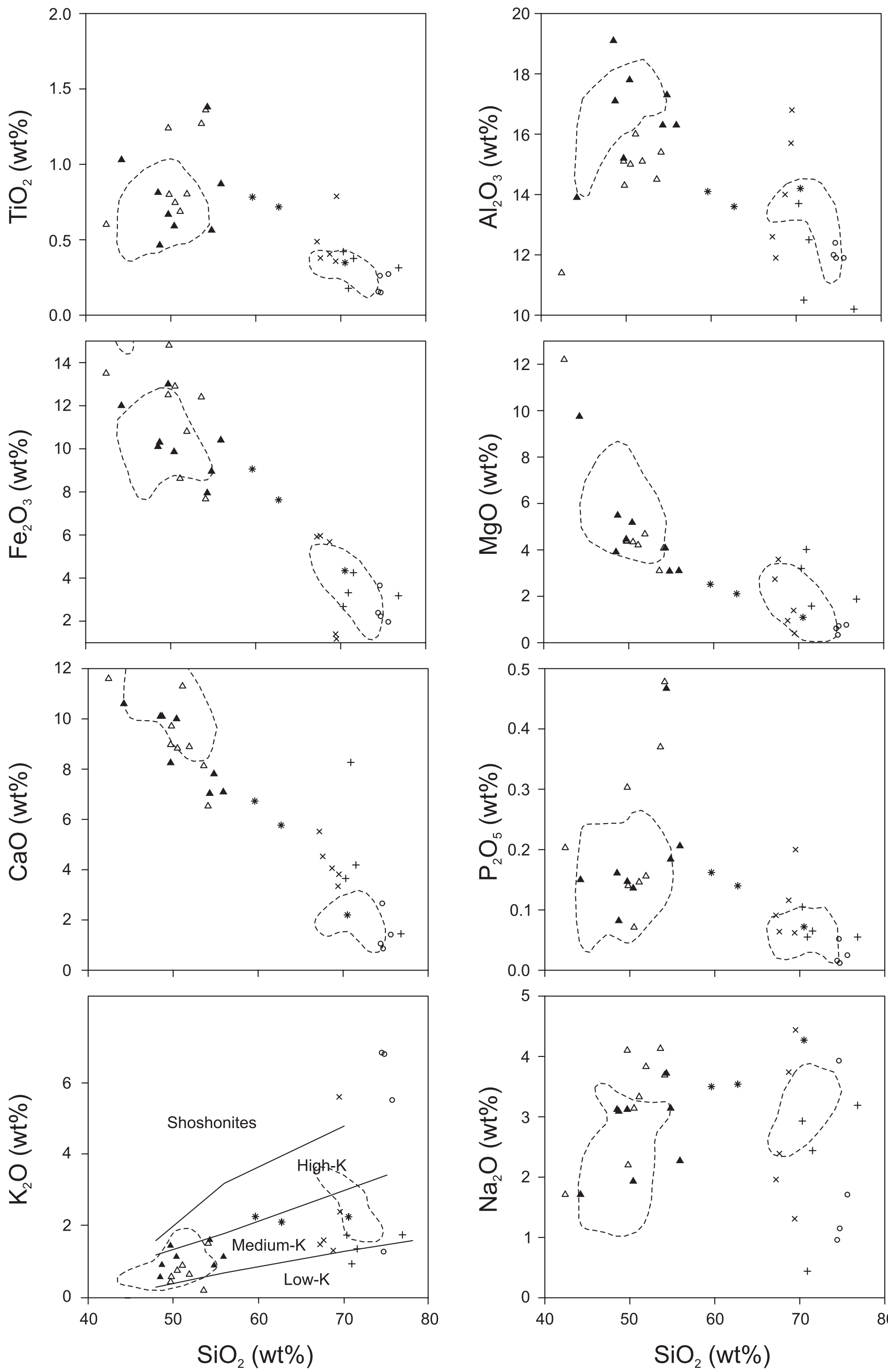

Fig. 5. Major elements vs. SiO_2 diagrams. The fields in SiO_2 vs. K_2O diagram after Peccerillo and Taylor (1979). For comparison, geochemical data of the Orijärvi formation samples (after Väisänen & Mänttäri, 2002) are presented in areas enclosed with dashed line (tot = 21 samples). One of the Orijärvi formation samples in both SiO_2 vs. MgO and SiO_2 vs. Al_2O_3 diagrams plots above the diagram. Symbols as in Fig. 4.

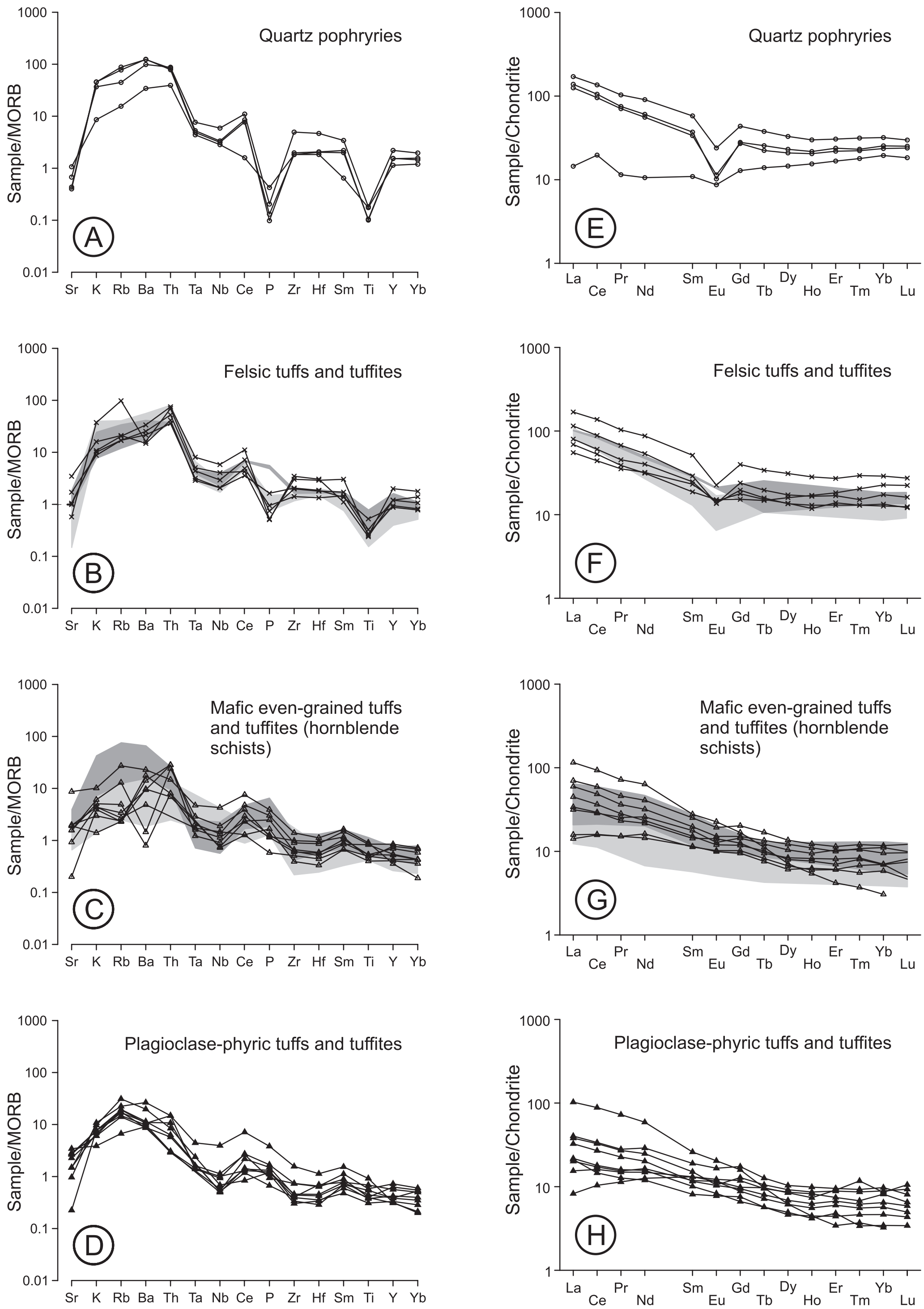

Fig. 6. MORB-normalized multi-element (a-d) and chondrite-normalized REE diagrams (e-h) of the Kuovila area rocks. Dark and light-coloured shading represent compositional fields of the rocks in the Kisko and Orijärvi formations, respectively (Väisänen & Mänttäri, 2002). Shading in b) and f) stand for felsic rocks and in c) and g) for mafic rocks. Normalizing values for MORB from Pearce (1983) and for chondrite from Boynton (1984). Symbols as in Fig. 4.

strength element (HFSE), rare earth element (REE), light rare earth element (LREE), heavy rare earth element (HREE), mid-ocean ridge basalt (MORB), and ocean island basalt (OIB). The LILE group contains mobile elements Cs, Rb, K, Ba, Sr and HFSE group contains less mobile elements Y, Hf, Zr, Ti, Nb, Ta and Ce.

All the Kuovila area felsic volcanic rocks show pronounced LREE enrichment and a flat HREE pattern with moderate enrichment in respect to chondritic values (Fig. 6). One of the quartz porphyries has a diverging REE pattern with remarkably lower LREE enrichment compared to the other felsic rocks (Fig. 6e). Felsic volcanic rocks generally show a flat HREE pattern and negative Eu-anomalies, the latter evidently resulting from plagioclase fractionation or plagioclase sustaining in the source residue (Rollinson, 1993). In contrast, the mafic volcanic rocks have a constant slope of the HREE pattern and no Eu-anomalies.

Multi-element spider diagrams of the felsic rocks show slightly higher relative enrichment of LILEs over HFSEs in comparison with the studied mafic rocks. This, together with depletion of Ti in the felsic samples is consistent with a fractional crystallization

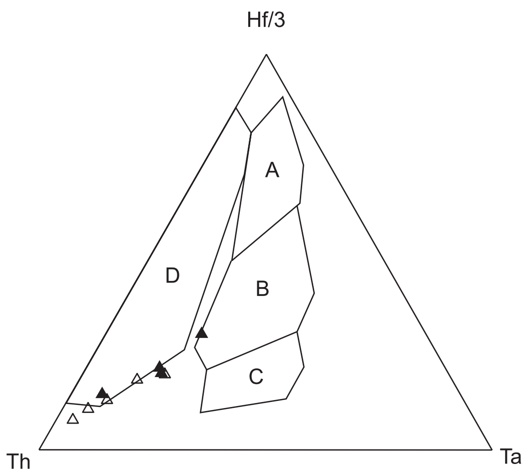

Fig. 7. Tectonic discrimination diagram for basalts after Wood et al. (1979). Key: A = mid-ocean ridge basalt (MORB), B = MORB + within plate basalt (WPB), C = WPB, D = volcanic arc basalt. Symbols as in Fig. 4.

trend from basalt to rhyolite (Pearce, 1996). According to Macdonald et al. (2000; and references therein), enrichment of LILEs relative to LREE and especially relative to HFSEs distinguishes arc magmas from those generated in other tectonic settings, such as MORB and OIB. The distinctive depletion of Nb and Ta in relation to Th and LREE in all the Kuovila area volcanic rocks indicates volcanic arc settings (Pearce, 1996). Tectonic discrimination diagram for basalts after Wood et al. (1979) also indicates that the Kuovila area mafic volcanic rocks have a volcanic arc affinity (Fig. 7). However, the plotted samples define a trend towards the within plate affinity field and are located at the base of the volcanic arc field, thus indicating geochemical processes typical for a collision zone (Fig. 10b, p. 105 in Pearce, 1996).

In comparison with the Orijärvi formation, REE contents of the Kuovila area mafic volcanic rocks are slightly higher, thus better correlating with the mafic rocks of the Kisko formation (Väisänen & Mänttäri, 2002). The multi-element diagram patterns of both the Kuovila area felsic and mafic rocks are, nevertheless, nearly identical with the patterns of the felsic and mafic rocks of the Orijärvi formation, respectively. Mafic rocks of the Kisko formation show a more pronounced enrichment of the LILEs compared to the Kuovila area mafic volcanic rocks.

All of the minor and trace element data together with the tectonic discrimination diagram for basalts suggest volcanic arc setting for the Kuovila area volcanism. In addition, major and trace element affinities support correlation of the Kuovila area volcanic rocks with the Orijärvi and Kisko formations, which are interpreted as having formed parts of the same volcanic arc (Väisänen & Mänttäri, 2002).

4. Geochronology

For U-Pb dating a sample from a layered, plagioclase bearing felsic tuff (A1658) was chosen. Zircons from sample Kuovila A1658 are mainly translucent and prismatic; their appearance being typical for magmatic zircons. Four zircon fractions consisting of similar, fine-grained (<75μm) zircons from two density frac-

Table 2. Multigrain TIMS U-Pb age data from Kuovila tuff, sample Kuovila A1658. Sample coordinates: 6670498N, 2466 051E (Finnish KKJ-2).

Sample information	Sample	U	Pb	$^{206}Pb/^{204}Pb$	$^{208}Pb/^{206}Pb$	ISOTOPIC RATIOS[1,2]			APPARENT AGES / Ma ± 2sigma		
Analysed mineral and fraction	weight/ mg	ppm		meas-ured	radio-genic	$^{206}Pb/^{238}U$	$^{207}Pb/^{235}U$	$^{207}Pb/^{206}Pb$	$^{206}Pb/^{238}U$	$^{207}Pb/^{235}U$	$^{207}Pb/^{206}Pb$
A) d>4.2,-200mesh, prismatic, translucent, abraded 21h	0.49	686	248	2533	0.12	0.333	5.299	0.116	1851	1869	1889±2
B) d>4.2,-200mesh, prismatic, translucent	0.59	576	200	1354	0.12	0.315	4.984	0.115	1764	1817	1878±2
C) d:4.2-4.0,-200 mesh, prismatic, trans-lucent,abraded 21h	0.61	913	320	2772	0.13	0.323	5.114	0.115	1802	1838	1880±2
D) d:4.2-4.0,-200mesh, prismatic,translucent	0.46	864	281	1446	0.11	0.297	4.677	0.114	1676	1763	1868±2

1) Isotopic ratios corrected for fractionation, blank (50 pg), and age related common lead (Stacey & Kramers 1975; $^{206}Pb/^{204}Pb$±0.2, $^{207}Pb/^{204}Pb$±0.1, $^{208}Pb/^{204}Pb$±0.2).

2) 2 sigma errors for Pb/U and $^{207}Pb/^{206}Pb$ ratios are 0.65% and 0.15 %, respectively. Error correlations between $^{206}Pb/^{238}U$ and $^{207}Pb/^{235}U$ ratios are 0.97.

Methods. The datings were performed at GTK, Espoo, Finland. The decomposition of zircons and extraction of U and Pb for multigrain TIMS age determinations follows mainly the procedure described by Krogh (1973). ^{235}U-^{208}Pb-spiked and un-spiked isotopic ratios were measured using a VG Sector 54 thermal ionization multicollector mass spectrometer. The measured lead and uranium isotopic ratios were normalized to the accepted ratios of SRM 981 and U500 standards. The Pb/U ratios were calculated using the PbDat-program (Ludwig, 1991) and the fitting of the discordia line as well as calculation of the intercept ages using the Isoplot/Ex 3 program (Ludwig, 2003).

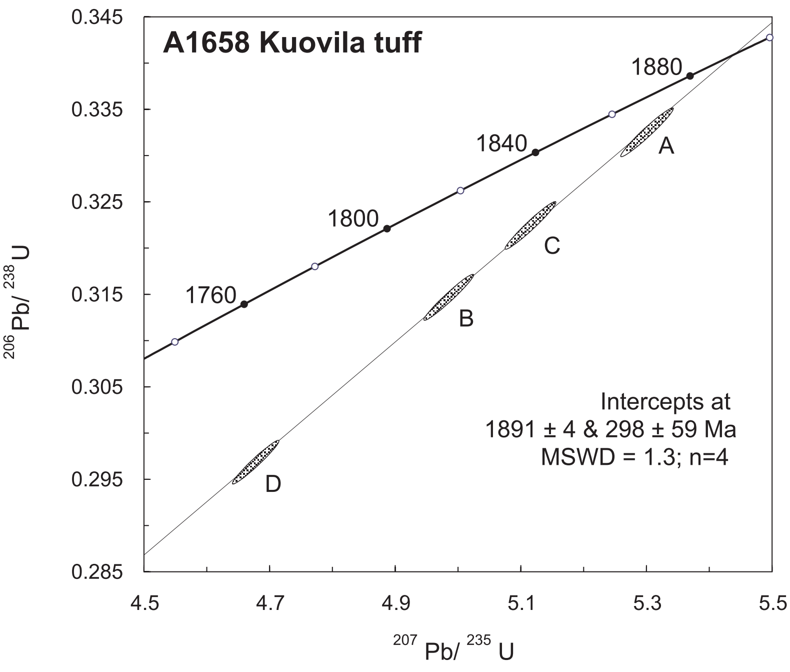

Fig. 8. U-Pb concordia diagram showing the age of the Kuovila tuff. Data point error ellipses are 2σ.

tions (d>4.2 gcm^{-3} and 4.2>d>4.0 gcm^{-3}) were analysed (Table 2). Two of the fractions were air-abraded. All the four analysed fractions plot well on a discordia line which intercepts the concordia curve at 1891.1±4 and 298±59 Ma (MSWD=1.3; n=4) (Fig. 8). The upper intercept age of 1891±4 Ma is considered to determine the age of volcanism in the Kuovila area.

5. Deformation structures

One regional scale prograde deformational event, D_2, with associated axial planar cleavage, S_2, folds S_0 and a weaker, layer-parallel S_1 cleavage (Fig. 2). S_1 has been preserved as inclusion trails within porphyroblasts and as a crenulated early cleavage in the F_2 fold hinges. The Kuovila area supracrustal rocks occur within an upright D_2 synform with a subhorizontal, curvilinear B_2 fold axis. The main cleavage (S_2) is subvertical and locally shows fanning across the F_2 fold hinges. D_2 deformation is locally partitioned into intensely folded high strain zones. Two separate phases of Svecofennian granitoids border the map unit of Kuovila on all sides except on the western side where the supracrustal units continue as part of the E–NE to W–SW trending Uusimaa Belt.

5.1. Description and relative timing of fabrics, metamorphism and intrusive phases

S_1 cleavage in the felsic volcanic rocks, subparallel to layering and defined by alignment of actinolite and biotite grains, is crenulated by F_2 folding with associated axial planar S_2 cleavage (Fig. 9a). S_1 is rarely visible in outcrop, while the main cleavage S_2 is generally well developed in mafic layers, but difficult to discern in the felsic quartz and feldspar rich layers (Fig. 9b). Locally, F_2 folds with gently plunging axes are associated with axial planar pressure solution cleavages (Fig. 9c). Discrimination between S_1 and S_2 cleavages in BIF is difficult due to the parallelism of the F_1 and F_2 axial planes on the limb of the large-scale F_2 fold, where the folded BIFs are located. Only one cleavage, axial planar to the folds in BIF (Fig. 9d) is recognized in a chert layer between magnetitic layers. The observed cleavage is either S_1, which has locally been preserved unaffected by later deformations within rheologically competent units, or S_2, in which case a) the pre-existing fabrics were destroyed by annihilation of the mineral grains after D_2, or b) no S_1 cleavage was developed. The latter alternative is favored by the presence of inclusion-free garnet porphyroblast cores in association with some BIFs and by the mineral composition in the BIF unit, unfavorable for preservation of the earlier fabrics.

Metamorphic mineral growth with respect to the cleavage development indicates two separate stages: garnet grains in a metamorphosed mafic rock grew over S_1 cleavage, now preserved as an internal S_1 cleavage within the porphyroblasts, oblique to the external main cleavage of the rock (S_2) (Fig. 9e). Thus, garnet growth was a late/post-D_1 and pre-D_2 event. Quartz grains in the garnet-bearing rock have been completely recrystallized in equilibrium conditions indicating heating concomitant with or post-dating D_2 deformation. It is suggested that there was one progressive metamorphic event, with increasing P and T from D_1 to peak metamorphic D_2. Partial melting conditions were, however, not reached.

The synvolcanic intrusive association is characterized by an intense tectonic foliation and strongly tectonized internal contacts subparallel to the main S_2 foliation. The granodiorites of the synvolcanic association contain abundant mafic magmatic enclaves (MMEs) of variable sizes and shapes. Felsic xenocrysts inside the MMEs indicate comagmatic origin for the rocks of the association (Fig 9f). The syn-D_2 granodiorite occurs in the hinge zone of the large F_2 fold in the eastern part of the study area. A porphyritic intermediate dyke, both truncating S_0 in a felsic volcanic and being included within the syn-D_2 granodiorite, provides clear evidence of the crosscutting relationships (Figure 9g). The both intrusives comprise an S_2 but no evidence of S_1. The granodiorite intrudes the layered volcanic rock both along S_0 and F_2 axial plane, thus indicating syn-D_2 origin. The intermediate dykes occur in the F_2 fold hinges, most

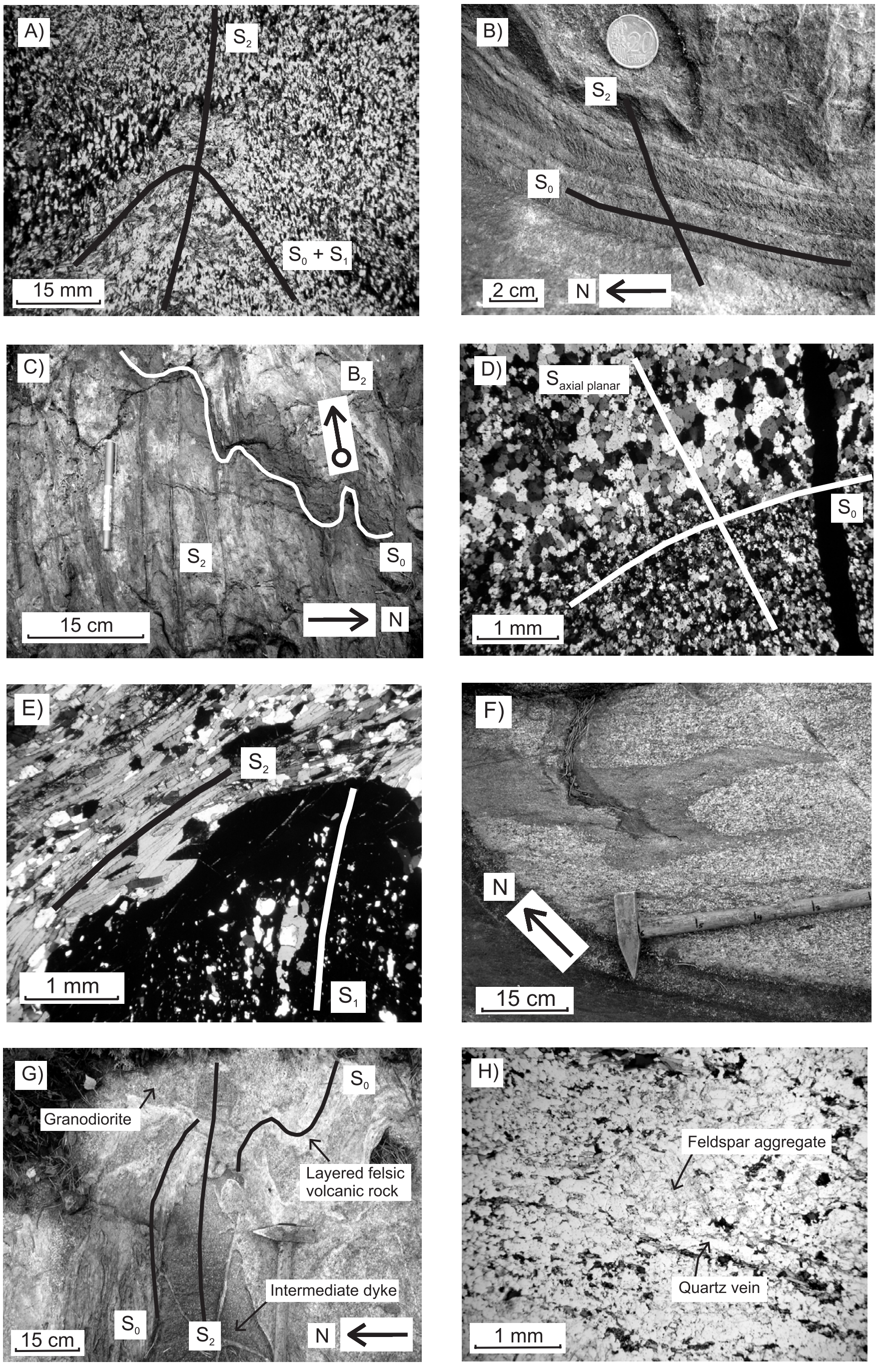

Fig. 9. Photomicrographs and outcrop photos. a) Photomicrograph of D_2 crenulated S_1 in the hinge of a F_2 fold with shallow B_2 axis. Outcrop is located in the hinge zone of the larger F_2 fold. Plane-polarized light (ppl). b) Well-developed S_2 cleavage in mafic layers in the hinge zone of the larger F_2 synform. c) Axial planar zonal S_2 pressure solution cleavage cross-cutting shallow S_0. d) Photomicrograph of a quartz-rich layer between magnetite-rich layers in a BIF exhibiting an axial planar cleavage. See text for origin of the cleavage. Cross-polarized light (cpl). e) Photomicrograph of pre-D_2 garnets with an internal S_1 foliation inclined to the external S_2 cleavage (cpl). f) Flow shapes and felsic xenocrysts within mafic magmatic enclaves in granodiorite indicating comagmatic origin for the rocks. g) A syn-D_2 granodiorite truncating both the S_2-foliated intermediate dyke and the layered felsic volcanic rock. Note the weak S_2 foliation in the granodiorite. Locality 46-PMSK-04 (6669976N, 2467072E, coordinates in Finnish KKJ-2). h) Photomicrograph of elongate quartz veinlets and sheared K-feldspar porphyroclasts in granodiorite (ppl).

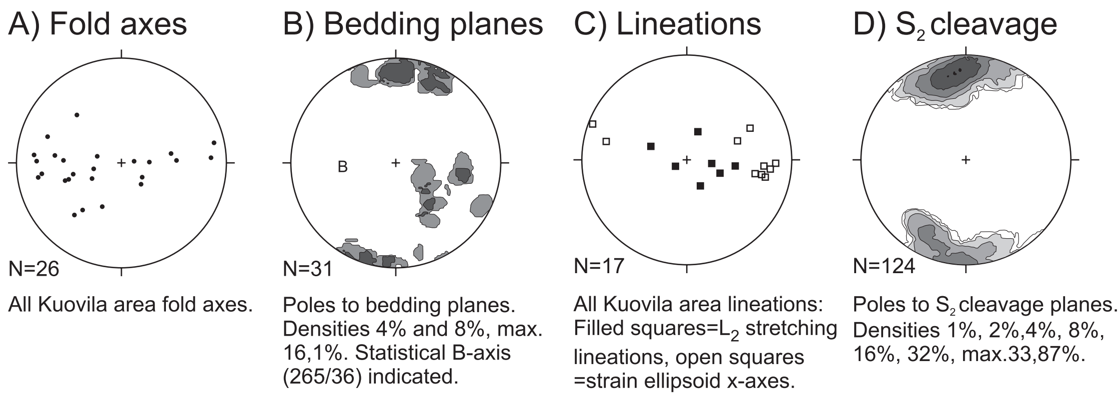

Fig. 10. Stereographic projections of the main structural elements of the study area (lower hemisphere, equal area projections).

probably indicating emplacement between D_1 and D_2, or early/syn-D_2. Another observation supporting the presence of two distinctly separate intrusive phases is where a granodiorite with less intense S_2 foliation intrudes strongly foliated older diorite comprising MMEs and inclusions of isoclinally folded layered felsic volcanic rocks.

The two granitoid phases exhibit rather similar microstructures: 1) grain aggregates of almost pure K-feldspar, sheared in a brittle/rigid style to produce sigma-shaped porphyroclasts, as revealed by boudinage of the clasts and associated, dynamically recrystallized quartz-rich tails (Fig. 9h). 2) Veinlets of quartz consisting of stretched elongate quartz grains, indicating medium-grade metamorphic conditions with temperatures between 400 and 700°C (Passchier & Trouw, 1996). The deformation microstructures in intrusive rocks are consistent with heating during or subsequent to the main deformation, recorded by the static equilibrium structures with triple junctions of 120-degree angles within the K-feldspar aggregates.

5.2. Geometry of the Kuovila area deformation structures

Geometry of the deformation structures in the study area is characterized by E–W trends on the large-scale F_2 fold limbs, and by closure of the fold in the east. Two discontinuous marble horizons act as lithological markers (Fig. 2). Fold axes in the area are subparallel in the map view, but show frequent changes in plunge, with both easterly or westerly plunges occurring within small areas (Fig. 2). The steep to subvertical fold axes plunge W–WSW whereas the gentler fold axes trend slightly more E–W (Fig. 10). The folds with steep axes generally occur as symmetric open folds with an S_0 enveloping surface at high angles to the strike of the D_2 axial planes on the outcrop scale (Fig. 11a). They are interpreted as D_2 -transposed F_1 folds within the D_2 low strain zone. Folds in the D_2 high strain zone have gentle, curvilinear axes. Bedding planes are tightly to isoclinally folded and boudinage occurs on the fold limbs (Fig. 11b). Figure 12 illustrates typical geometry of folding with variable fold axial plunges in a D_2 high strain zone. In conclusion, regional geometry of the supracrustal rocks at Kuovila indicates D_1 folded bedding planes prior to D_2 folding. The absence of well-developed S_1 cleavages indicates either moderate intensity or localization of D_1 folding or that D_1 occurred in a low-T regime, with little mineral growth. Small-scale D_1 thrust planes are found locally. Bedding planes in the F_2 fold hinge generally have shallow to moderate westerly dips with some steeper values present, too (Fig. 10). Statistically defined B-axis thus stands for an average of the curvilinear B_2 axis.

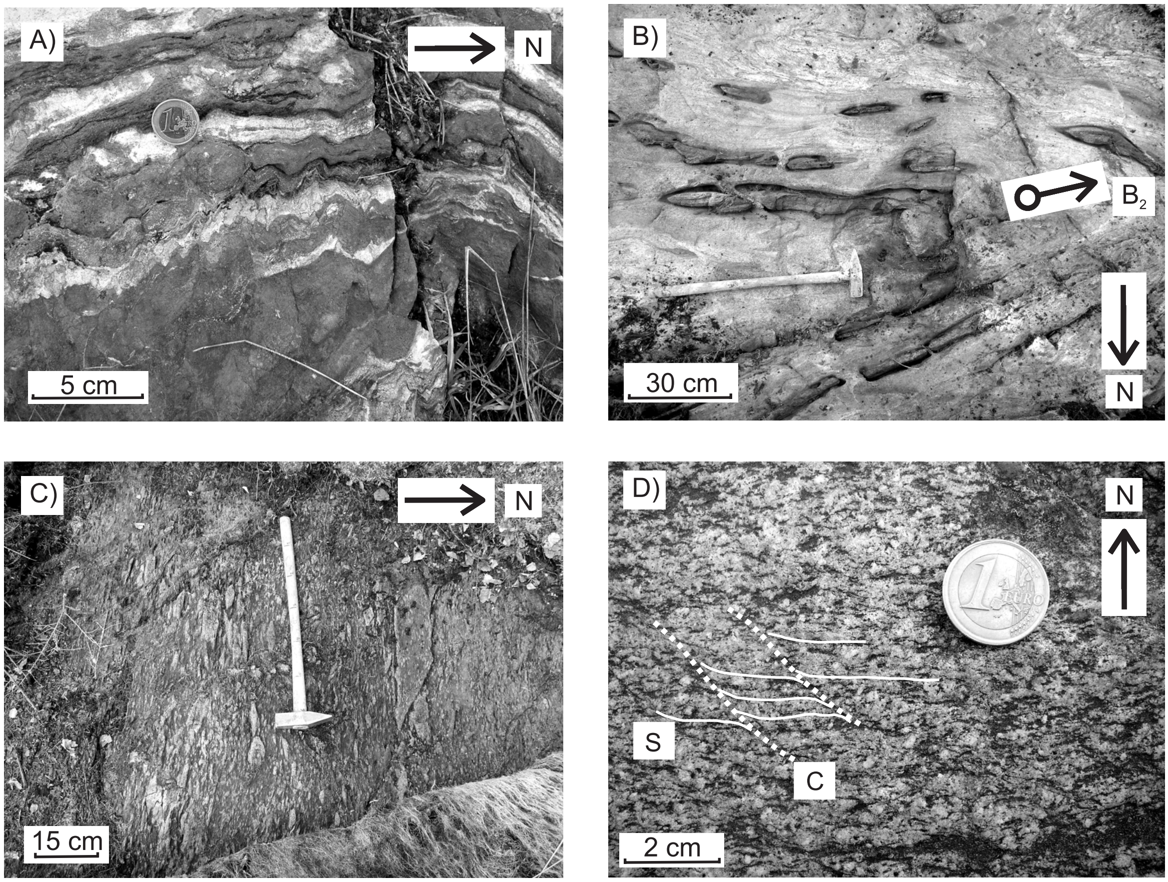

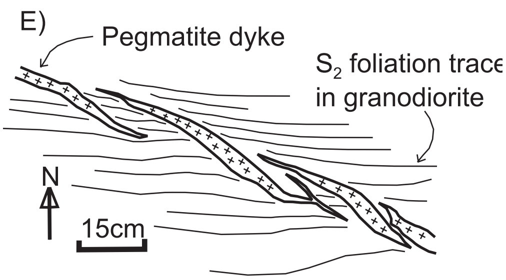

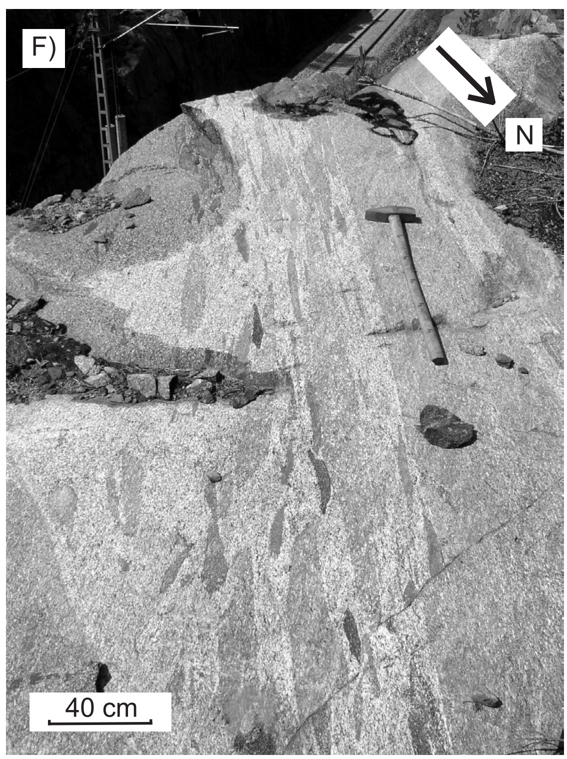

Fig. 11. Outcrop photos. a) An open, m-symmetric F_1 fold with steep axis. b) F_2 fold with a shallow fold axis plunging W in D_2 high strain zone. Bedding planes are boudinaged on the fold limbs. Mineral composition of the rock is unfavourable for the development of a strong S_2 cleavage. c) Volcaniclastic conglomerate formation with strained fragments, XZ plane of the strain ellipsoid in a zone of a higher cumulative strain within the conglomerate. d) Dextral S/C fabric in granodiorite. e) Pegmatite dykes intruding a granodiorite of the synvolcanic intrusive association (line drawing). f) Intensely strained enclaves of variable composition in the synvolcanic granodiorite.

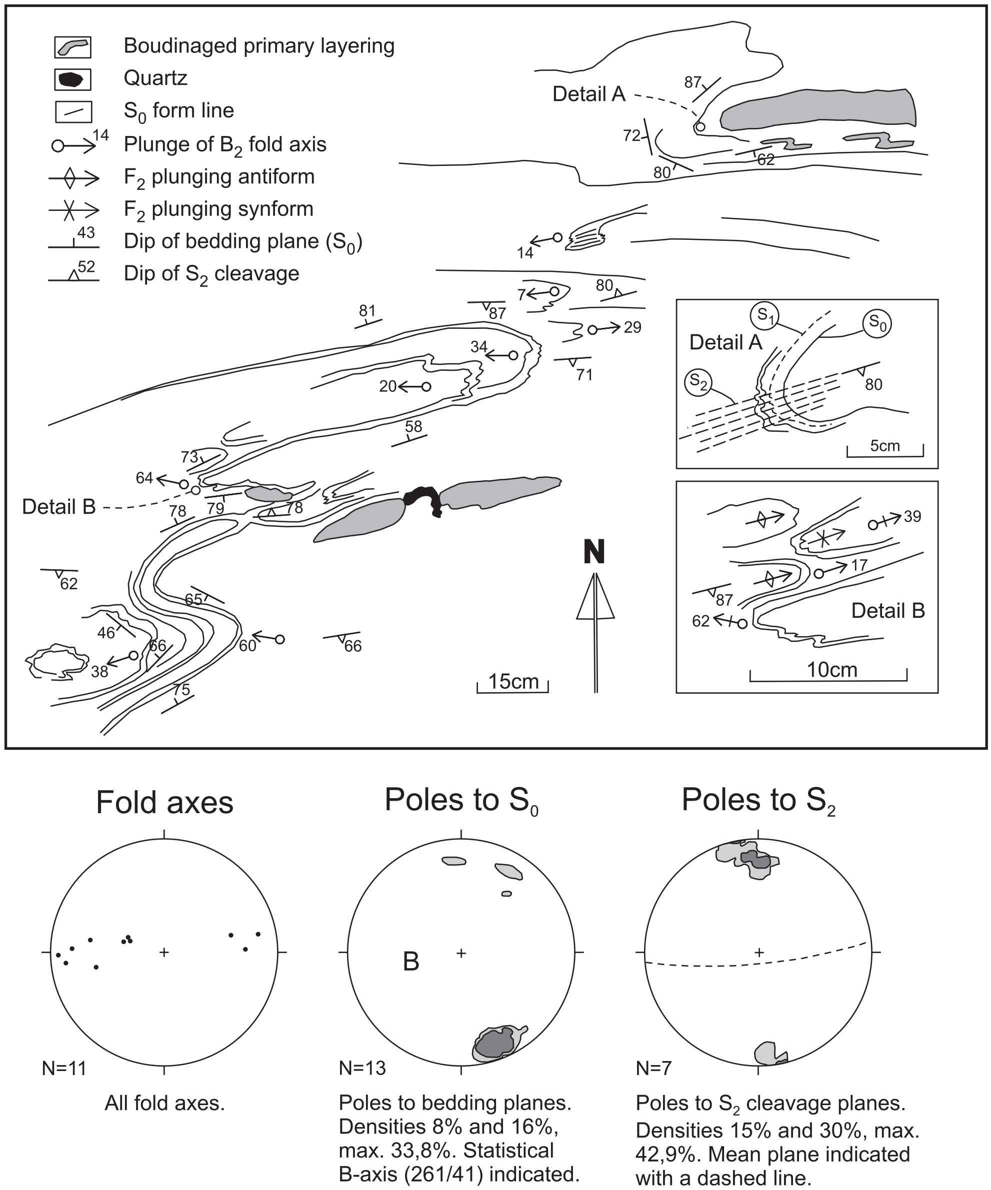

Fig. 12. Detailed map of folding in D_2 high strain zone with stereoplots of the associated structural elements. Note the variation in plunges of the fold axes. Locality 39-PMSK-04 (6670017N, 2466920E, coordinates in Finnish KKJ-2).

6. Discussion

6.1. Structural evolution, strain partitioning and deformation kinematics

Three lines of evidence suggest recumbent F_1 folds overprinted by upright F_2 folds:

1) The map pattern, where the folded marble horizons most probably are fragments of a single polydeformed layer. Strong attenuation and boudinage of the layer on fold limbs and thickening and buckling in the fold hinges probably took place both during D_1 and D_2. Absence of outcrop scale fold interference structures suggests large F_1 fold amplitudes compared to the F_2 folds, and a rather uniform, flat-lying F_1 fold limbs prior to D_2. 2) Stereographic analysis of the fold axes (Fig. 10a): The presently steep fold

axes were originally subhorizontal B_1 fold axes trending NNE to SSW, now rotated into steep orientation about the gently plunging regional B_2 fold axes. 3) Local, small-scale D_1 thrusts, suggesting thrusting towards ESE may have accompanied the F_1 folding. The principal stretch axes (X) in the zones of the highest cumulative strain, defined by strained fragments in the conglomerates, are subparallel to the gentle regional fold axes (Fig. 10). The X-axis orientation, however, probably indicates tectonic transport direction during D_1, which likely was perpendicular to the axes of the thrust-related, recumbent F_1 folds. Fragments within volcaniclastic conglomerate unit indicate moderate flattening strains with average aspect ratios of approximately (x: y: z) = 2.5: 2: 1. It is likely that the XY plane represents transposed S_1/S_2 cleavage plane, subparallel to S_2 orientation in the nearby volcanic and sedimentary units, with some intensifying of the fabric during D_2. Locally, constrictional strains with prolate clast shapes occur in specific locations (Fig. 11c).

Tavela (1950) also described early layer-parallel deformation structures from the Kuovila area. In relation to Svecofennian orogenic evolution elsewhere, early thrusting is consistent with the previous studies (van Staal & Williams, 1983; Bleeker & Westra, 1987; Ehlers et al., 1993). However, tectonic transport directions are variable as Ehlers et al. (1993) describes early folds overturned to the north and west, van Staal & Williams (1983) thrusting towards north, whereas the present study suggests thrusting towards SSE. Therefore, regional kinematics of the earliest tectonic stages in orogenic scale remains poorly constrained.

Some D_1 structures and fabrics are possibly preserved as a result of spatial D_2 strain variation with partitioning into axial planar high strain zones on the limbs of the large-scale F_2 fold and low strain domains in between. The low strain domains occur in the F_1 hinge zones within the rheologically competent units, such as BIFs, which have been acting as nearly rigid blocks that have mainly been "passively" rotated into their present position during D_2 with only minor "internal" strain. Thus, the main reason for the spatial D_2 strain variation would be the spatial distribution and geometry of the competent rheological units at the onset of D_2 stage.

D_2 of the Kuovila area probably correlates with the first tectonometamorphic event with associated migmatization and forming of the first penetrative fabric at ca. 1.88 Ga in the southern SSAC (Hopgood et al., 1983), but has taken place at higher crustal levels not involving migmatization. This is also favored by the absence of K-feldspar rich granites associated with migmatizing veins in the Kuovila area, characteristic for the 1.84–1.81 Ga event (Nironen, 2003). Deformations during the 1.84–1.81 Ga event also fold the main fabric of the rocks, whereas the Kuovila area supracrustals have the main fabric in the F_2 axial planes, similar to the Orijärvi triangle (Plogsma & Westra, 1990). Thus, combined with the very similar lithological and geochemical characteristics, D_2 deformation structures within the Kuovila area most probably correlate with D_1 of Ploegsma & Westra (1990). The possibility of the Kuovila area D_2 being related to the 1.84–1.81 Ga event, may, however, not be reliably ruled out without an absolute age determination for D_2 in the Kuovila area.

D_2 folds are resulting from horizontal, approximately N–S contraction. The curvilinear patterns of the B_2 fold axes probably result from vertical stretching perpendicular to the B_2 axes during D_2, associated with steep mineral aggregate lineations in the syn-D_2 granodiorite (Fig. 10). One possibility for the variation of the fold axial plunges would be refolding of F_2 folds. No evidence for such folding is however present in the Kuovila area. Location of the area bounded between NE–SW and NW–SE trending regional high strain zones has likely inhibited post-D_2 deformation in the Kuovila area, as in the Orijärvi low-strain triangle (Ploegsma & Westra, 1990). Therefore, it may be concluded that vertical movements, considered at least partly responsible for the doming of the Svecofennian Mustio dome (Härme, 1953; Bleeker & Westra, 1987; Veenhof & Stel, 1991) took place already during D_2 of the Kuovila area, now suggested to correlate with D_1 of the earlier studies (Bleeker & Westra, 1987; Ploegsma & Westra, 1990), thus predating the doming at Mustio.

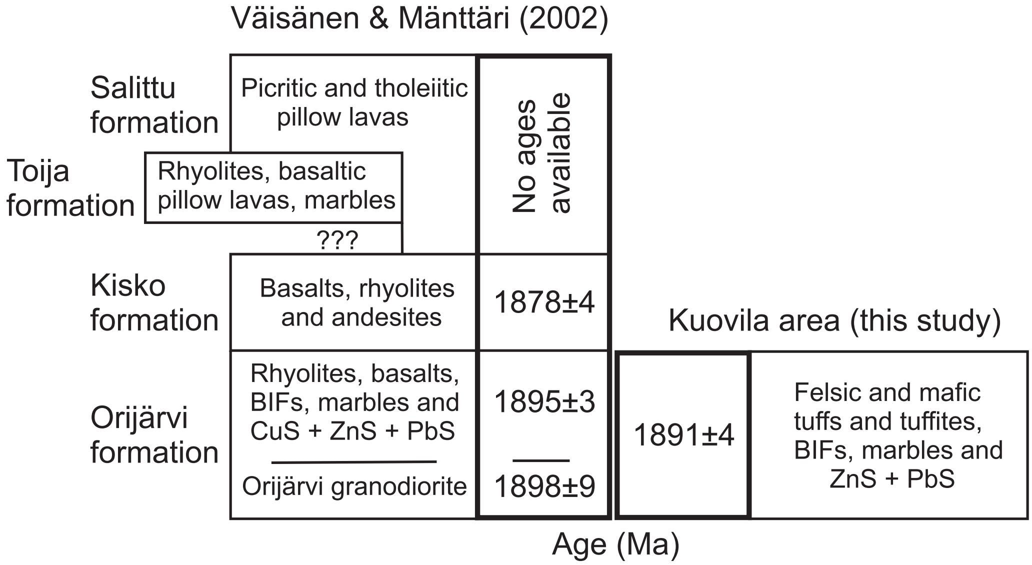

Fig. 13. Correlation of the Kuovila area rocks with the stratigraphy of the Orijärvi area (Väisänen & Mänttäri, 2002).

Origin of the dextral S/C fabrics in the synvolcanic granodiorite (Fig. 11d) either results from shearing or oblique overprinting of S_2 over S_1, as do the dextral en-echelon arrays in pegmatite veins intruding the granodiorite (Fig. 11e). Weak, gently plunging lineations related to shearing in the granodiorite would indicate dextral, mainly strike-slip movements along E–W trending shear zones, thus consistent with the regional interpretation of transpressive deformation deforming the ~ 1.84–1.83 Ga old granites within the SSAC (Ehlers et al., 1993). Localization of cumulative strain in the synvolcanic intrusive association, revealed by variably flattened MMEs in different parts of the intrusive (Fig. 11f), is also suggested to relate to the strike-slip shearing, possibly during the vaning stages of the orogeny at ~ 1.8 Ga.

6.2. Regional geotectonic correlation

Geochemical data show a distinct similarity between the Kuovila area and the Orijärvi and Kisko formations described by Väisänen & Mänttäri (2002). The Kisko formation, however differs lithologically from the Kuovila and the Orijärvi areas, which both comprise BIFs, marbles (Eskola, 1914; Mäkelä, 1989; Keinänen, 1980) and sulphide mineralizations sharing very similar ZnS-PbS-CuS distributions (Mäkelä, 1989; Käpyaho, 2001). The amount of sulphide mineralization and the degree of hydrothermal alteration are higher at Orijärvi.

Age of the volcanism is 1895±3 Ma in the basal parts of the Orijärvi formation, 1878±Ma at higher stratigraphical level in the Kisko formation (Väisänen & Mänttäri, 2002) and 1891±4 Ma for the Kuovila felsic tuff. Within error limits, these ages in the Kuovila and Orijärvi are therefore contemporaneous. These features suggest that these areas can probably be correlated (Fig. 13). However, the wider main element distribution and the higher REE contents of the former in some respects resemble also the Kisko and Salittu formations overlying the Orijärvi formation (Väisänen & Mänttäri, 2002). The volcanic rocks of the Kuovila area and the Orijärvi formation represent the earliest identified volcanic stage in the southern Svecofennian Uusimaa Belt, also being concurrent with the Bergslagen area of south-central Sweden (Lundström et al., 1998).

The possible correlation of the D_2 in the Kuovila area with the early deformation structures pre-dating the metamorphic peak and the associated S-type granites at ~ 1.84–1.82 Ga elsewhere in the Uusimaa Belt, possibly implies two separate structural successions. These both would be characterized by very similar deformational events including early recumbent, thrust-related folds overprinted by upright E–W trending folds caused by N–S crustal contraction (e.g. Schreurs & Westra, 1986; Ehlers et al., 1993). It is also possible that the structural succession within the Kuovila area represents deformation structures related to the ~ 1.84–1.82 Ga event, but at higher crustal levels, not including partial melting. This is, however, not favoured by the granodioritic composition of the syn-D_2 intrusive in the Kuovila area. Anyhow, dating of the structural events both in the migmatitic and non-migmatitic domains of the SSAC will be needed to discriminate between the structural successions related to the older and the younger tectonothermal events.

7. Conclusions

1. Volcanism in the Kuovila area is geochemically similar to the modern-day volcanic arc environment and similar to the stratigraphically lowermost volcanic rocks in the Orijärvi area. A felsic tuff in the Kuovila area, dated at 1891±4 Ma by U-Pb isotopes analyzed on zircons, is contemporaneous with volcanic rocks in the Orijärvi formation. Thus, the Kuovila area volcanic rocks and the Orijärvi formation represent the same stage and approximately the same stratigraphical horizon in the evolution of Southern Svecofennian Arc Complex.

2. Approximately horizontal N–S contraction during the peak metamorphic D_2 resulted the upright F_2 folds now defining the Kuovila synform. D_2 is associated with axial planar S_2 cleavages and curvilinear B_2 fold axes. D_2 strain is partitioned into low strain domains and narrow high strain zones. Metamorphic conditions did not reach partial melting during D_2. D_1 structures probably were low metamorphic and localized, thrust-related recumbent folds with large amplitudes.

3. Emplacement of a granodioritic intrusive phase took place syntectonic with D_2 deformation.

Acknowledgements

We wish to thank staff at the geochemistry laboratory at the Geological Survey of Finland (GTK) for the geochemical analyses, Marita Niemelä at the isotope laboratory at GTK and mineral separation staff for heavy liquid mineral separation. Andrej Wennström and Jouko Pääkkönen prepared the thin sections. Jarmo Kohonen, Peter Sorjonen-Ward and one anonymous referee is thanked for critical reviews of the manuscript, and Petri Peltonen for the editorial handling of the manuscript. Rod Holcombe is thanked for a critical review of an earlier version of the manuscript. Discussions with Mikko Nironen and Timo Kilpeläinen were instructive. Pentti Hölttä helped with the metamorphic matters during the work. Nick Oliver pointed out several important details in the field and in thin sections. Jukka Reinikainen and Olli Sarapää are acknowledged for cooperation in the early stages of the project. Pekka Karimerto and Jukka Kaunismäki are thanked for assistance in sampling. Colleagues at GTK are acknowledged for inspiring discussions. The National Graduate School of Geology and GTK funded this work.

References

Allen, R.L., Lundström, I., Ripa, M., Simeonov, A. & Christofferson, H., 1996. Facies analysis of a 1. 9 Ga, continental margin, back-arc. Felsic caldera province with diverse Zn-Pb-Ag-(Cu-Au) sulphide and Fe oxide deposits, Bergslagen Region, Sweden. Economic Geology 91, 979–1008.

Bleeker, W. & Westra, L., 1987. The evolution of the Mustio gneiss dome, Svecofennides of SW Finland. Precambrian Research 36, 227–240.

Gorbatshev, R. & Bogdanova, S., 1993. Frontiers in the Baltic Shield. Precambrian Research 64, 3–21.

Boynton, W.V., 1984. Geochemistry of the rare earth elements: meteorite studies. In: Henderson, P. (ed.) Rare earth element geochemistry. Elsevier, p. 63–114.

Colley, H. & Westra L., 1987. The volcano-tectonic setting and mineralization of the early Proterozoic Kemiö-Orijärvi-Lohja belt, SW Finland. In: Pharaoh, T.C., Beckinsale, R.D., Rickard, D. (eds.) Geochemistry and mineralizations of Proterozoic volcanic suites. Geological Society Special Publications 33, 95–107.

Ehlers, C., Lindroos, A. & Selonen, O., 1993. The late Svecofennian granite-migmatite zone of southern Finland-a belt of transpressive deformation and granite emplacement. Precambrian Research 64, 295–309.

Ekdahl, E., 1993. Early Proterozoic Karelian and Svecofennian formations and the evolution of the Raahe-Ladoga ore zone, based on the Pielavesi area, central Finland. Geological Survey of Finland, Bulletin 373, 137 p.

Eskola, P., 1914. On the petrology of the Orijärvi region

in southwestern Finland. Bulletin de la Commission Géologique de Finlande 40, 277 p.
Eskola, P., 1915. On the relations between the chemical and mineralogical composition in the metamorphic rocks of the Orijärvi region. Bulletin de la Commission Géologique de Finlande 44, 145 p.
Eskola, P.E., Hackman, V., Laitakari, A. & Wilkman, W.W., 1919. Suomen kalkkikivi. Geologisen komission geoteknisiä julkaisuja N:o 21, 265 p. (in Finnish).
Gaál, G., 1990. Tectonic styles of early Proterozoic ore deposition in the Fennoscandian Shield. Precambrian Research 46, 83–114.
Hietanen, A., 1975. Generation of potassium-poor magmas in the northern Sierra Nevada and Svecofennian of Finland. Geological Society of America Bulletin 58, 1019–1085.
Hopgood, A.M., Bowes, D.R., Kouvo, O. & Halliday, A.N., 1983. U-Pb and Rb-Sr isotopic study of polyphase deformed migmatites in the Svecocarelides, southern Finland. In: Atherton, M.P. & Gribble, C.D. (eds.) Migmatites, melting and metamorphism. Shiva, Cheshire. 80–92.
Huhma, H., 1986. Sm-Nd, U-Pb and Pb-Pb isotopic evidence for the origin of the Early Proterozoic Svecokarelian crust in Finland. Geological Survey of Finland, Bulletin 337, 48 p.
Härme, M., 1953. Structure and stratigraphy of the Mustio area, southern Finland. Bulletin de la Commission Géologique de Finlande 166, 29–48.
Jurvanen, T., Eklund, O. & Väisänen, M., 2005. Generation of A-type granitic melts during the late-Svecofennian metamorphism in southern Finland. GFF 127, 139–147.
Keinänen, V., 1980. Orijärven alueen rautakerrostumista. M.Sc. Thesis, University of Turku, Finland (in Finnish), 85 p.
Koistinen, T., 1992. Tammisaari. Explanation to the Geological map of Finland 1:100 000, pre-Quarternary rocks, sheet 2014, 10 p (in Finnish).
Korsman, K., Korja, T., Pajunen, M., Virransalo, P. & GGT/SVEKA Working group, 1999. The GGT/SVEKA Transect: Structure and Evolution of the Continental Crust in the Paleoproterozoic Svecofennian Orogen in Finland. International Geology Review 41, 287–333.
Krogh, T.E., 1973. A low-contamination method for hydrothermal decomposition of U and Pb for isotopic age determinations. Geochimica et Cosmochimica Acta 37, 485–494.
Kurhila, M., Vaasjoki, M., Mänttäri, I., Rämö, T. & Nironen, M., 2004. Conventional and ion-probe U-Pb results on the lateorogenic microcline granites in southern Finland. In: Mansfeld, J. (ed.) The 26th Nordic Geological Winter Meeting, Uppsala, Sweden. GFF 126, 27.
Käpyaho, A., 2001. Pohjan Kuovilan karbonaattikivien esiintymisympäristön petrologia ja geokemia.. M.Sc. Thesis, University of Helsinki, Finland (in Finnish), 74 p.
Latvalahti, U., 1979. Cu-Zn-Pb Ores in the Aijala-Orijarvi area, Southwest Finland. Economic Geology 79, 1035–1059.
Le Bas, M.J., Le Maitre, R.W. Streckeisen, R. & Zanettin, B., 1986. A Chemical Classification of Volcanic Rocks Based on the Total Alkali-Silica (TAS) Diagram. Journal of Petrology 27, 745–750.
Levin, T., Engström, J., Lindroos, A., Baltybaev, S. & Levchenkov, O., 2005. Late-Svecofennian transpressive deformation in SW Finland – evidence from late-stage D3 structures. GFF 127, 129–137.
Ludvig, K.R., 1991. PbDat 1.21 for MS-dos: A computer program for IBM-PC Compatibles for processing raw Pb-U-Th isotope data. Version 1.07. U.S. Geological Survey Open-File Report, 88–542, 35 p.
Ludwig, K.R., 2003. Isoplot/Ex 3. A geochronological toolkit for Microsoft Excel. Berkeley Geochronology Center. Special publication No. 4.
Lundström, I., & Papunen, H., (eds.) 1986. Mineral deposits of soutwestern Finland and the Bergslagen province, Sweden. Sveriges Geologiska Undersökning, Ser. Ca 61. 44 p.
Lundström, I., Allen, R.L., Persson, P-O. & Ripa, M., 1998. Stratigraphies and depositional ages of Svecofennian, Palaeoproterozoic metavolcanic rocks in E. Svealand and Bergslagen, south central Sweden. GFF 120, 315–320.
Macdonald, R., Hawkesworth, C.J. & Heath, E., 2000. The Lesser Antilles volcanic chain: a study in arc magmatism. Earth-Science Reviews 49, 1–79.
Mouri, H., Väisänen, M., Huhma, H. & Korsman, K., 2005. Sm–Nd garnet and U–Pb monazite dating of high-grade metamorphism and crustal melting in the West Uusimaa area, southern Finland. GFF 127, 123–128.
Mäkelä, U., 1983. On the geology of the Aijala-Orijärvi area, southwest Finland. In: Laajoki, K. & Paakkola, J. (eds.) Exogenic processes and related metallogeny in the Svecokarelian geosynclinal complex. Guide to field trips for the IGCP Projects 91 and 160 in eastern, central and southern Finland, August 17-26, 1983. Geological Survey of Finland, Guide 11, 140-160.
Mäkelä, U., 1989. Geological and geochemical environments of Precambrian sulphide deposits in southwestern Finland. Annales Academi Scientiarum Fennicae III 151, 102 p.
Nironen, M., 1997. The Svecofennian orogen: a tectonic model. Precambrian Research 86, 21–44.
Nironen, M., 2003. Renewed classification of Proterozoic orogenic granitoid rocks in Finland. In: Rämö, O.T., Kosunen, P.J., Lauri, L.S. & Karhu, J.A. (eds.) Granitic Systems – State of Art and Future Avenues. An International Symposium in Honor of Professor Ilmari Haapala, January 12–14, 2003, Abstract Volume. Helsinki University Press, 120 p.
Passchier, C.W. & Trouw, R.A.J., 1996. Microtectonics. Springer Verlag, Berlin. 289 p.
Pearce, J.A., 1983. Role of subcontinental lithosphere in

magma genesis at active continental margins. In: Hawkesworth, C.J. & Norry, M.J. (eds.) Continental Basalts and Mantle Xenoliths. Nantwich: Shiva, 230–249.

Pearce, J.A., 1996. A User`s Guide to Basalt Discrimination Diagrams. In: Wyman, D.A. (ed.) Trace Element Geochemistry of Volcanic Rocks: Applications for Massive Sulphide Exploration. Geological Association of Canada, Short Course Notes, vol. 12, 79–113.

Pearce, J.A., Harris, N.B.W. & Tindle, A.G., 1984. Trace element discrimination diagrams for the tectonic interpretation of granitic rocks. Contributions to Mineralogy and Petrology 25, 956–983.

Peccerillo, R. & Taylor, S.R., 1976. Geochemistry of Eocene calc-alkaline volcanic rocks from the Kastamonu area, northern Turkey. Contributions to Mineralogy and Petrology 58, 63–81.

Ploegsma, M. & Westra, L., 1990. The Early Proterozoic Orijärvi triangle (southwest Finland): a key area on the tectonic evolution of the Svecofennides. Precambrian Research 47, 51–69.

Reinikainen, J., 2001. Petrogenesis of paleoproterozoic marbles in the Svecofennian domain, Finland. Geological Survey of Finland, Report of investigation 154, 84 p.

Rollinson, H.R., 1993. Using Geochemical Data: Evaluation, Presentation, Interpretation. Longman, Essex. 352 p.

Schreurs, J. & Westra, L. 1986. The thermotectonic evolution of a Proterozoic, low pressure, granulite dome, West Uusimaa, SW Finland. Contributions to Mineralogy and Petrology 93, 236–250.

Sipilä, P., 1981. Lounais-Suomen rautamalmeista. M.Sc. Thesis, University of Turku, Finland (in Finnish), 106 p.

Simonen, A., 1953. Stratigraphy and sedimentation of the Svecofennidic, early Archean supracrustal rocks in South-Western Finland. Bulletin de la Commission Géologique de Finlande 160, 37–64.

Stacey, J.S. & Kramers, J.D. 1975. Approximation of terrestrial lead isotope evolution by a two-stage model. Earth and Planetary Science Letters 26, 207–221.

Suominen, V., 1991. The chronostratigraphy of southwestern Finland with special reference to Postjotnian and Subjotnian diabases. Geological Survey of Finland, Bulletin 356, 100 p.

Tavela, M., 1950. Havaintoja Kuovilan alueelta Kiskon-Kemiön leptiittivyöhykkeellä. M.Sc. Thesis, University of Helsinki, Finland (in Finnish), 57 p.

Tuominen, H., 1957. The structure of an Archean area: Orijärvi, Finland. Bulletin de la Commission Géologique de Finlande 177, 32 p.

van Staal, C.R. & Williams, P.F., 1983. Evolution of a Svecofennian-mantled gneiss dome in SW Finland, with evidence for thrusting. Precambrian Research 21, 101–128.

Verhoef, P.N.W. & Dietvorst, E.J.L, 1980. Structural analysis of differentiated schists and gneisses in the Taalintehdas area, Kemiö Island, southwest Finland. Bulletin of the Geological Society of Finland 52, 147–164.

Väisänen, M., and Mänttäri, I., 2002. 1.90–1.88 Ga arc and back-arc Basin in the Orijärvi area, SW Finland. Bulletin of the Geological Society of Finland 74, 185–214.

Väisänen, M., Mänttäri, I. & Hölttä, P., 2002. Svecofennian magmatic and metamorphic evolution in sothwestern Finland as revealed by U-Pb zircon SIMS geochronology. Precambrian Research 116, 111–127.

Wood, D.A., Joron, J-L. & Treuil, M., 1979. A re-appraisal of the use of trace elements to classify and discriminate between magma series erupted in different tectonic settings. Earth and Planetary Science Letters 45, 326–336.